CHEMISTRY OF MATERIALS

Article

pubs.acs.org/cm

Micro-, Mesoporous Boron Nitride-Based Materials Templated from Zeolites

S. Schlienger,[†] J. Alauzun,[‡] F. Michaux,[§] L. Vidal,[†] J. Parmentier,*[,†] C. Gervais,[§] F. Babonneau,[§] S. Bernard,[⊥,]* P. Miele,[⊥] and J. B. Parra[#]

[†]Institut de Science des Matériaux de Mulhouse, LRC CNRS 7228, Université de Haute Alsace, 15 rue Jean Starcky, BP 2488, 68057 Mulhouse Cedex, France

[‡]Institut C. Gerhardt, CMOS, Université Montpellier II, CC1701, Place Eugène Bataillon, 34095 Montpellier Cedex 5, France

[§]Laboratoire de Chimie de la Matière Condensée de Paris UMR CNRS 7574, UPMC, Collège de France, 11 place M. Berthelot, 75005 Paris, France

[⊥]Institut Européen des Membranes de Montpellier (UMR CNRS 5635), Université Montpellier II, CC047, Place Eugène Bataillon, 34095 Montpellier Cedex 5, France

[#]Instituto Nacional del Carbón, CSIC, Apartado 73, 33080 Oviedo, Spain

Supporting Information

ABSTRACT: A second generation of boron nitride-based porous materials has been synthesized by a double nanocasting process via a carbonaceous template as a medium starting from a zeolite. In the multistep process, we coupled several synthetic strategies such as chemical vapor deposition (CVD) and polymer-derived ceramic (PDCs) routes to prepare carbonaceous templates through infiltration of zeolite Y (FAU structure type) by propylene in the gaseous phase then infiltration of the carbonaceous replica having a high micropore volume (0.67 cm^3/g) with polyborazylene in the liquid phase followed by pyrolysis and mold destruction. These porous BN-based architectures present a bimodal pore size distribution with a high portion of micropores (~0.20 cm^3/g) that are unambiguously evidenced by nitrogen physisorption based on a nonporous BN reference isotherm. They exhibited a high specific area (570 m^2/g), a high pore volume (0.78 cm^3/g), and a lack of long-range ordering as evidenced by BET, XRD and TEM experiments. The two first properties allow to open catalyst applications of these materials.

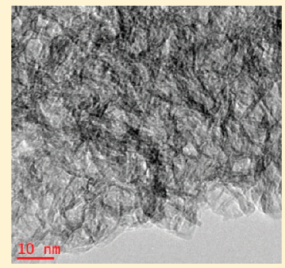

KEYWORDS: *porous boron nitride, micropore, mesopores, nanocasting, zeolite template, polyborazylene, t-plot*

INTRODUCTION

The hexagonal phase of boron nitride (h-BN) is isostructural to graphite and is the stable phase at room temperature (RT) and ambient pressure. It attracts increasing interest because of its properties suitable for a wide range of applications. It offers the lowest density (d = 2.26 $g.cm^{-3}$) among nonoxide ceramics, a chemical inertness with molten metals, excellent optoelectronic properties, a relatively good thermal stability, in particular in air, as well as specific structural properties such as high thermal conductivity, electrical insulation and lubricating properties.[1−5] However, BN is only produced as powders (mainly plate-like morphology), coatings and workpieces. In order to develop new industrial applications of BN, it is required to create materials with controlled shape (fibers, coatings, composites) and morphologies (dense, micro/meso/macroporous) as it has been intensively developed for carbon materials. However, the preparation of these type of BN materials needs the development of new chemical methods such as the relatively recent polymer-derived ceramics (PDCs) route. It is based on the shaping then pyrolysis of preceramic polymers into ceramics with controlled shapes[6−8] and morphologies.[9−11] Even if it is not well developed at industrial scale, this route can provide materials with a direct application in industry as demonstrated by Clariant,[12] Dow Corning,[13] and Starfire systems.[14]

Among materials with a high industrial impact, porous materials hold a significant position as attested by their widespread use in several industrial processes and household products. Generally, these materials arise only from modified natural materials (e.g., activated carbons...) or from oxide synthetic materials (e.g., zeolites). Applications of microporous or mesoporous materials (pore size below 2 nm and between 2 and 50 nm respectively) are therefore mainly restricted to these two families of materials. However, there are needs for new compositions especially based on nonoxide. BN may be one of the appropriate candidates. It can propose application in corrosive environments and microelectronics where the widely investigated oxide and/or sulfide ceramics cannot work properly. In particular, we think that it is a valuable alternative to porous silica beads as supported noble metals catalysts for removal exhaust gas pollutants or for activity in CO oxidation reactions.[15]

Received: July 7, 2011
Revised: September 9, 2011
Published: December 9, 2011

dx.doi.org/10.1021/cm201938h | *Chem. Mater.* 2012, 24, 88−96

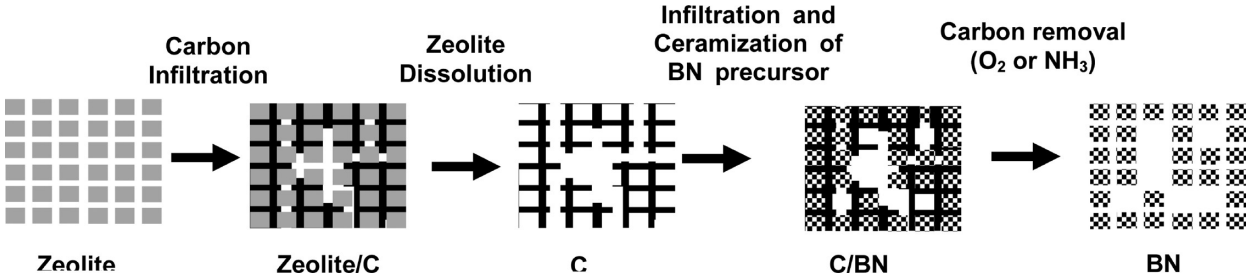

Figure 1. Overall synthetic path employed to generate zeolite-derived BN-based materials with micro- and mesoporosity. Note that the last structure is in fact disorganized.

The hard-template methodology is well fitted for the preparation of porous BN.[16,17] It allows for the control of both pore dimension and pore size distribution. Combined with the PDCs route, the hard-template methodology makes use of preformatted, hard and porous templates impregnated with a preceramic polymer to generate porous ceramics after subsequent pyrolysis in oxygen-free atmosphere then destruction of the mold.[16−24] Whereas bi- or trimodal porosity is required for catalyst supports, only BN powders with monodisperse pore size distribution, mainly mesoporous, have been produced up to now by the hard template methodology.[17]

Herein, we report the preparation of BN-based materials with a high surface area and a hierarchical bimodal porosity. This second generation of porous BN materials has been prepared by a double nanocasting process via a zeolite-templated carbon replica, as schematized in Figure 1. The preparation of these intermediate carbon materials, first developed by Kyotani starting with zeolite Y (FAU- structure type)[25,26] has more recently been extended to other zeolite-structure types such as BEA[27−29] or EMT.[30−33] These materials display an ordered nanostructured and a signification microporosity (up to 1.4 cm^3/g) far above most of commercial activated carbon materials. They have therefore promising applications in separation processes[34] and for H_2 or CH_4 storage.[35] but as far as the authors' knowledge, they have never been used as hard templates for the nanocasting process. Infiltration of their porosities with a polyborazylene, precursor of BN, has led here to a novel zeolite-derived BN-based architecture in which micropores were clearly evidenced for the first time besides mesopores. Such materials display potential applications in many fields as adsorbents, energy storage media, and catalyst supports.

EXPERIMENTAL SECTION

Materials. The polyborazylene is unstable in air. Therefore, all manipulations were carried out under inert conditions. Argon (>99.995%) was purified by passing through successive columns of phosphorus pentoxide, siccapent, and BTS catalysts. Schlenks were dried at 120 °C overnight before pumping under vacuum and filling them with argon for synthesis. Manipulation of the chemical products was made inside an argon-filled glovebox (Jacomex BS521; Dagneux, France) dried with phosphorus pentoxide.

Polymer Synthesis. The operating procedure to prepare borazine was reported in our previously published paper.[36] Polyborazylene, labeled **PB**, has been synthesized to impregnate the porous structure of the carbonaceous template. 17.8 g of borazine were introduced at 0 °C in a 75 mL autoclave (from Equilabo, France) with a temperature and pressure controller (Parr N 4836 Model) in an argon-filled glovebox using Teflon-Lining to easily remove the polymer from the autoclave. Borazine was gradually heated to 60 °C (1 °C min^{-1}), then kept at this temperature until stabilization of the internal pressure. The process created a final internal pressure of 121.1 bar after a dwelling time of ∼240 h. The condensation of borazine generated significant amounts of H_2 which were carefully removed from the autoclave after cooling down to room temperature (RT). Then, the autoclave was introduced inside an argon-filled glovebox to recover ∼15.2 g of a white powder with a yield of 85% in weight. Chemical analysis, IR and NMR characterization data of polyborazylene are reported below.Anal. Found (wt %): B, 37.46; N, 56.47; H, 5.26; O, 0.79 $[B_{3.0}N_{3.5}H_{4.5}O_{0.04}]_n$ ($[86.63]_n$). IR (KBr/cm^{-1}): ν(N−H) = 3445 m; ν(B−H) = 2509 m; ν(B−N) = 1435 s; δ(B−N−B) = 890 m; δ(BH) = 690 m. ^{11}B MAS NMR (128.28 MHz/ppm): δ = 31 (BN_2H), 27 (BN_3). TGA (N_2, 1000 °C, 90.9% ceramic yield): 25−70 °C: Δm = 0%; 70−280 °C: Δm = 4.5%; 290−750 °C: Δm = 3.5%; 750−1000 °C: Δm = 1.1%.

Preparation of the Carbonaceous Replica of Zeolite. Microporous zeolite-templated carbon replica was prepared using a three-step procedure derived from the one reported by Kyotani et al.[26] Five grams of dried zeolite Y (FAU type) was first heated up to 800 °C under argon atmosphere in the vertical furnace. At this dwell temperature, the porosity of the zeolite was infiltrated with carbon during 2 h by chemical vapor deposition using an argon-propylene mixture (2.5% of propylene). A heat-treatment at 900 °C during 4 h under argon was then carried out to stabilize the negative carbonaceous replica confined into the porous structure of zeolite. The as-obtained zeolite-carbonaceous composite was immersed in hydrofluoric acid (40 wt %) at RT in PTFE systems, and then washed thoroughly with deionized water. Around 1 g of material was recovered after a drying step at 100 °C for 12 h. The zeolite-carbonaceous replica labeled **C** was characterized by chemical analysis, nitrogen physisorption at 77 K and X-ray diffraction.

Preparation of the Zeolite-Derived Boron Nitride-Based Architecture. The nanocasting step was carried out through an impregnation process in a Schlenk type flask. The microporous carbon, dehydrated at 150 °C for 4 h under reduced pressure (5×10^{-2} mbar) prior to use, was first impregnated with a 10 wt % in THF solution of **PB** (300 mg). The mixture was kept unstirred for 24 h at room temperature under static vacuum. The Schlenk-type glass containing the mixture was heated up to 50 °C under reduced pressure and held at this temperature for 2 h in order to remove THF. The temperature was then increased up to 200 °C and kept 2 h to initiate the cross-linking of **PB**. Finally, the system was allowed to cool to RT under constant flow (50 mL min^{-1}) of argon and the as-prepared composites were then transferred into an alumina tube inserted in a horizontal tube furnace. Subsequently, the sample was subjected to a cycle of ramping of 1 °C min^{-1} to 1200 °C, dwelling there for 2 h (with a constant nitrogen volumetric flow of 0.039 m^3 s^{-1} through the tube), and then cooling to RT at 5 °C min^{-1} to give a composite sample. The latter was then shared into two parts. A first part underwent a thermal treatment in ammonia from RT to 1000 °C overnight to remove the carbon template, while generating the sample labeled **BN-1200-NH_3** where 1200 °C is the ceramization temperature and NH_3 the gas used for the carbon template removal. A second part was subjected to another cycle of ramping of 5 °C min^{-1} to 1450 °C (2 h, with the same nitrogen volumetric flow and cooling process). It underwent a thermal treatment in ammonia from RT to 1000 °C overnight which was completed by a second treatment in air from RT to 600 °C (5 °C min^{-1} with a dwelling time of 4 h) to fully remove the carbon template and give the sample labeled **BN-1450-O_2**.

dx.doi.org/10.1021/cm201938h | *Chem. Mater.* 2012, 24, 88−96

The BN samples, **BN-1200-NH_3** and **BN-1450-O_2**, have been characterized by elemental analysis, solid-state NMR, XRD, SEM, TEM, and N_2 physisorption.

Characterizations. Bulk compositional evolution of samples was made in the Service Central de Microanalyse de Vernaison (Vernaison, France) for hydrogen, boron, carbon, nitrogen, and oxygen. The methods included thermal decomposition of powders under oxygen to measure carbon and hydrogen contents, under inert atmosphere for the measurement of nitrogen and oxygen contents and by ICP for boron content. In addition, powders were analyzed by energy-dispersive X-ray (EDX). The samples were observed by transmission electron microscopy (TEM, FEI-Philips CM200) and by scanning electron microscopy (SEM, FEI-Quanta 400). The X-ray diffractograms were collected with an Xpert Pro Panalytical with Cu Kα_1 radiation (λ = 0.15406 nm).

^{11}B MAS NMR spectra were recorded at 11.75 T on a Bruker Avance500 wide-bore spectrometer operating at 128.28 MHz, using a Bruker 4 mm probe and a spinning frequency of the rotor of 14 kHz. The spectra were acquired using a spin−echo $\theta-\tau-2\theta$ pulse sequence with θ = 90° to overcome problems of probe signal. The τ delay was synchronized with the spinning frequency and recycle delay of 1s was used. Chemical shifts were referenced to $BF_3(OEt)_2$ (δ = 0 ppm). Spectra were fitted using the DMFIT program.[37]

The nitrogen physisorption isotherms were recorded at 77 K on a Micromeritics ASAP 2420 after outgassing samples at 300 °C during 15 h. Specific surface areas (S_{BET}) were calculated using the relative pressure range where a linear representation of the modified Brunauer−Emmett−Teller (BET) equation proposed in ref 38 is obtained (here 0.01−0.10). Micropores were evidenced by the Dubinin−Radushkevich (DR) and t-plot methods. The latter method required the isotherm of a nonporous BN reference material. Because of the absence of relevant data in the literature, the isotherm of such BN sample was recorded. That material, obtained by a self-propagating high-temperature synthesis, has a specific surface area of 3.6 m^2/g. Although this sample displays a type-II adsorption isotherm, its nonporous feature was checked with the Frenkel−Hasley−Hill (FHH) equation,[39] $V_{ads,ref} = (K/\ln(P_0/P))^{1/H}$ where $V_{ads,ref}$ is the adsorbed volume for this reference material and H the coefficient of the FHH equation. The fitted H value, 2.71, was closed to the 2.70 value expected for a good nonporous standard material. The statistical adsorbed layer thickness t (nm) was then calculated with the following equation, t = 0.354 $V_{ads,ref}/V_{monolayer,\ ref}$, where $V_{monolayer,\ ref}$ is the volume obtained from the statistical monolayer derived from the BET surface area for that reference material.[40] t values for different relative pressures are given in Table 2 in the Supporting Information. The multilayer thickness t versus relative pressure was also fitted with polynomial eqs 1 and 2 in the relative pressure ranges 0−0.01 and 0.01−1 respectively.

$$t = -63217(P/P_0)^4 + 10204(P/P_0)^3\text{-}2828(P/P_0)^2 + 36,09(P/P_0) \quad (1)$$

$$t = 25,55(P/P_0)^5 - 56,22(P/P_0)^4 + 45,93(P/P_0)^3 - 16,83(P/P_0)^2 + 3,410(P/P_0) + 0,106 \quad (2)$$

The total pore volumes were obtained at a relative pressure P/P_0 of 0.95. The pore size distribution was determined with the NLDFT method (Micromeritics software) considering carbon adsorbent and slit-shaped pore geometry.

RESULTS AND DISCUSSION

Preparation of the Zeolite-Derived BN-Based Architectures. In the multistep process depicted in Figure 1, we coupled several synthetic strategies such as sol−gel, CVD and PDCs routes to prepare functional BN-based architectures with a bimodal micro- mesopore size distribution and a significant pore volume. These enhanced properties, compared to those of traditional or nanocasted BN materials, are related to the use of the zeolite-derived carbon replica which displays a high ratio of micropores. The latter was obtained by using a single carbon infiltration step of zeolite Y (CVD of propylene) avoiding thus a time-consuming double step infiltration process usually necessary for the preparation of faithful carbon replicas displaying a well ordered microporosity.[30,41] It allows to prepare easily one gram of carbon material per batch while preserving microporosity and a high surface area (see below). This high surface area is stabilized by a large portion of heteroatoms, mainly oxygen atoms present up to 9 wt %.[42] It should be mentioned that we decided to infiltrate the carbonacesous replica rather that the zeolite template due to the temperatures that are fixed during the preparation of BN (1200 and 1450 °C). Indeed, for such high temperatures, the zeolite structure collapses.

Because of the fact that the molecular origin of preceramic polymers is a key parameter that predetermines the shape and the properties of PDCs, the choice of the preceramic polymer is a first crucial factor that affects the preparation of porous PDCs. Based on its properties, polyborazylene fulfills the particular requirements to control the various demands with respect to processing of porous BN. It is synthesized with controlled cross-linking degrees by self-condensation of borazine at low temperature inside an autoclave under static argon. Borazine represents a source of both boron and nitrogen elements with the correct boron-to-nitrogen ratio and symmetry. It is liquid, unstable at RT and has a tendency to completely evaporate during the further ceramic conversion by heat-treatment.[43] This fact prevents the preparation of porous BN by liquid-phase infiltration then heat-treatment inside the porous structure of the carbonaceous replica. Thus, the key step to produce porous BN is to control the thermal reactivity of borazine allowing it to be confined in the carbonaceous replica in a stable process, then transformed into BN by heat-treatments without collapsing of the porous structure. The strategy by which this can be accomplished is to polymerize the borazine into a RT-stable polymer called polyborazylene before infiltration. We have recently focused on the synthesis of polyborazylene to prepare boron nitride shapes including nanotubes[36] and workpieces[44] by tuning the operating parameters of the polyborazylene synthesis. The physical state, viscosity, and ceramic yield of polyborazylene are tuned by the temperature of the self-condensation of borazine. A polyborazylene prepared by self-condensation of borazine below 50 °C is liquid but remains unstable at RT. It is required to self-condense the borazine at 50 °C to generate a liquid compound that remains stable at RT for several weeks.[36] This polymer has been first used to infiltrate the zeolite-templated carbonacesous replica but, it was required to adjust its viscosity by dilution in THF to enhance the infiltration process of the carbonaceous template which can be simply estimated from the yield and densities. However, the ceramic yield of this polyborazylene (50.3% measured under nitrogen atmosphere after decomposition at 1000 °C) was too low to replicate the carbonaceous template and we obtained a materials with large voids in the pore walls generating a relatively large porosity, and in turn a large pore volume with a monomodal porosity (mainly mesoporous) which finally fits the process of infiltrating CMK-3 template.[17] Within this context, it is required to use a polyborazylene that exhibits a relatively high ceramic yield to replicate the carbonaceous template. A thermolysis of borazine at 60 °C generated a solid polyborazylene labeled **PB**, ($[B_{3.0}N_{3.5}H_{4.5}]_n$; oxygen values were found to be lower than 2 at % and were therefore omitted[44]) which is soluble in THF. The viscosity of the as-obtained solution can be adjusted, e.g., a solution of **PB**

dx.doi.org/10.1021/cm201938h | Chem. Mater. 2012, 24, 88−96

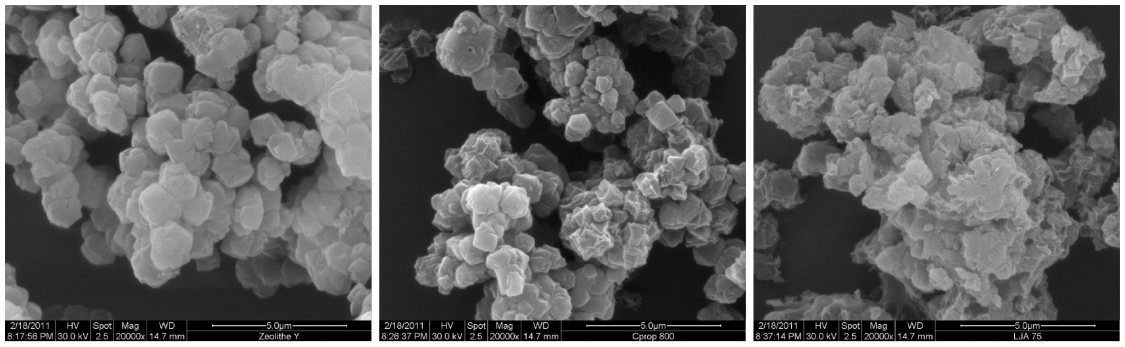

(a) (b) (c)

Figure 2. SEM images of samples (a) zeolite Y, (b) zeolite-templated carbon replica **C** and (c) BN replica **BN-1200-NH$_3$**.

in a 10 wt % in THF is ideal to infiltrate the zeolite-templated carbonaceous replica before removing THF at low temperatures (50 °C) under reduce pressure. Furthermore, it displays a very high ceramic yield (90.9%), which avoids both the collapse of the structure during the polyborazylene-to-boron nitride conversion and the formation of large voids in the pore walls.

The second crucial factor is the nanocasting-pyrolysis-carbon removal cycle. Table 1 in the Supporting Information summarizes the different experimental conditions used for ceramization or the template removal with some of the corresponding properties of the materials obtained. The number of infiltration-pyrolysis-carbon removal cycles has to be fixed to optimize the loading amount of **PB** to be confined in the carbonaceous template. For comparison, two samples have been prepared according to one and two infiltration-ceramization cycles (see Table 1 in the Supporting Information). Interestingly, the second cycle decreases the BET surface and the pore volume of the material most probably because a large excess of **PB**; thereby BN does not infiltrate the template after the first infiltration-pyrolysis cycle and remains at the surface of the carbonaceous template. Furthermore, the removal of the carbon template is more difficult (12 wt % remains) because of the fact that BN acts as a passivating layer around the carbonaceous replica. This was also the case by combining a solid **PB** in the first cycle and the liquid one (synthesized by self-condensation of borazine at 50 °C) for the second cycle. Within this context, we only applied one infiltration-pyrolysis-carbon removal cycle with **PB** synthesized at 60 °C. It should be mentioned that a duration of 10 h under ammonia is required to eliminate completely the carbon after a ceramization at 1200 °C for 2 h (sample **BN-1200-NH$_3$**). This duration could be reduced using air at 600 °C instead of ammonia or should be considerably increased (>20 h) if ceramization takes place at higher temperature. In the latter case, the higher density of the C/BN composite associated with the passivating effect of BN onto C delay probably the carbon removal. Moreover, trials with a highly microporous zeolite carbon replica (C-AF-Prop sample presented in Table 1 in the Supporting Information) leads to a difficult carbon removal of the C/BN composite. It is believed that its low fraction of mesopores precludes an indeed PB infiltration into its porosity and promotes BN deposition on the external surface of the composite with subsequent passivation of the carbon template.

The thrid crucial factor that affects the properties of porous ceramics in nonoxide systems is their expected relatively high sensitivity to oxygen according to their high specific surfaces. Studies of bulk polymer-derived BN have demonstrated that chemical inertness and in particular air-sensitivity is mainly controlled by the crystallinity of these materials.[44,45] The latter is adjusted usually by the final temperature of the process. Nevertheless, if a highly porous material is targeted, an increase of its crystallinity would be associated to a grain growth by a sintering process. The resulting decrease in its porosity by densification of the material would then be at the opposite of the targeted properties. Moreover, the sintering process could be strongly restricted according to the fact that BN preparation takes place in confined media (mainly within the microporosity of the carbon template). Therefore, a relatively high level of crystallinity combined with high nanoporosity seems difficult to achieve. To investigate this aspect, we have prepared two porous BN samples at 1200 and 1450 °C before elimination of the carbonaceous template. For the porous BN sample prepared at 1200 °C, the carbonaceous template elimination was performed under ammonia at 1000 °C for 10 h as previously mentioned leading to the sample labeled **BN-1200-NH$_3$**. Whereas this treatment was efficient to completely remove the carbonaceous template (see chemical analyses below) through a carbothermal reaction according to eq 1, it was required to perform a further treatment in air for the complete elimination of the carbonaceous template in the porous BN sample prepared at 1450 °C leading to **BN-1450-O$_2$**.

$$3C + 4NH_3 \rightarrow 3CH_4 + 2N_2 \quad (1)$$

It is believed that the **C/BN-1450** composite is denser than the **C/BN-1200** one and therefore less prone to promote diffusion of gas (e.g., NH_3) within its restricted porosity. The carbon removal under ammonia is then slowdown.

Thus, only BN samples (**BN-1200-NH$_3$** and **BN-1450-O$_2$**) resulting from optimized experimental procedures were investigated in the following of this publication.

SEM Observations. Representative micrographs of the zeolite Y labeled **FAU-Y**, the carbonaceous replica **C** and the zeolite-derived **BN-1200-NH$_3$** are shown in Figures 2a-c, respectively.

For the boron nitride replicated material **BN-1200-NH$_3$**, the crystalline morphology observed for the zeolite and its carbon replica (Figure 2a, b, respectively) is partly maintained although the particles appear to the glued together with an extra BN phase (Figure 2c). It suggests that a part of the PB has not been infiltrated into the carbon porosity.

Similar observations have been made for the sample **BN-1450-O$_2$**.

dx.doi.org/10.1021/cm201938h | *Chem. Mater.* 2012, 24, 88–96

Chemical Analyses and Solid-State NMR. Elementary analyses have been performed on both BN samples. Data are reported in Table 1.

Table 1. Chemical Compositions of Samples BN-1200-NH_3 and BN-1450-O_2 by Elemental Analysis

samples	H (at %)	C (at %)	O (at %)	N (at %)	B (at %)
BN-1200-NH_3	19	1	14	30	36
BN-1450-O_2	18	1	15	30	36

On the basis of our expertise in the synthesis of nanostructured boron nitride[36,43,44] and taking into account the severe problems associated with conventional elemental analyses (by combustion) of nitride,[22,24,43] we investigated elemental analyses and EDX analysis during SEM observations for boron, carbon, nitrogen, and oxygen contents. For EDX, we first calibrated with commercially available BN (from HC Starck) based on the composition given by the manufacturer. EDX results highly reflected measurements made by elemental analyses. As a consequence, we have given results obtained from elemental analyses. First, boron is in excess in comparison to nitrogen, which is usually observed for BN because the volatility of nitrogen is larger than that of boron.[43] Second, we observed a large ratio of oxygen within samples. We suggest that the O content level of the samples is due to either the interaction of **PB** with the carbonaceous template, which contains around 9 wt % oxygen[42] through oxygen-containing functional groups (e.g., ether, phenol, acid anhydride) or/and to the high reactivity in air of highly porous BN materials. We measured an empirical formula $B_{1.0}N_{0.85}C_{0.03}O_{0.4}H_{0.5}$ for both samples that can be assimilated to: $B_{1.0}N_{0.85}C_{0.03}O_{0.15}{\cdot}0.25H_2O$ or to $0.85BN/0.03C/0.15B(OH)_3$. Third, the low concentration of carbon trapped within the samples demonstrates the efficient carbon template elimination by ammonia for the sample **BN-1200-NH_3** which has been completed with air-treatment for the sample **BN-1450-O_2**. Carbon is not identified by Raman spectroscopy and samples are homogeneously white.

Here, we investigated solid-state NMR to identify the boron environment in our samples. ^{11}B solid-state NMR spectrum of samples **BN-1200-NH_3** and **BN-1450-O_2** (Figure 3) shows a large signal in the region of tricoordinated boron atoms that was tentatively simulated with two sites at 31 ppm (quadrupolar coupling constant C_Q = 2.9 MHz, η = 0.3) and 20 ppm (C_Q = 2.7 MHz, η = 0.1) assigned to B−N bonds in planar BN_3 groups[44−46] within BN graphitic layers and trigonal BO_3, respectively.

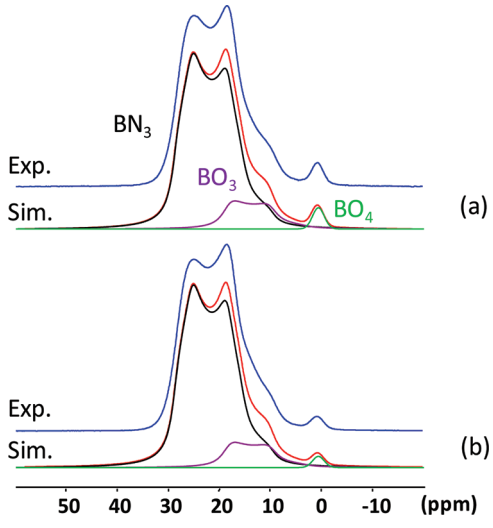

Figure 3. Experimental and simulated solid-state ^{11}B MAS NMR spectra of (a) **BN-1200-NH_3** and (b) **BN-1450-O_2**.

The second small signal at δ_{iso} = 0.6 ppm (no quadrupolar shape) is indicative of the presence of tetragonal BO_4 groups[47−49] in minor quantity.

NMR indicates that the reactivity toward oxygen originates from boron atoms. The relative intensities of the different types of boron environments are summarized in Table 2.

Table 2. Chemical Shift (reference: $BF_3(OEt)_2$) and Relative Intensity of the Different Types of Boron Environments

	site		
	BN_3	BO_3	BO_4
δ_{iso} (^{11}B) (ppm)	30.0	20.0	0.6
C_Q (MHz)	2.9	2.7	
η	0.3	0.1	
	signal intensity (±1%)		
BN-1200-NH_3	85	13	2
BN-1450-O_2	87	12	1

The relative amount of BO_x sites is less than 15% in both samples in good agreement with the chemical analysis for both samples.

N_2 Physisorption. We have first investigated the porosity of both BN samples in the micropore and mesopore ranges by N_2 physisorption measurements at 77 K (Figure 4).

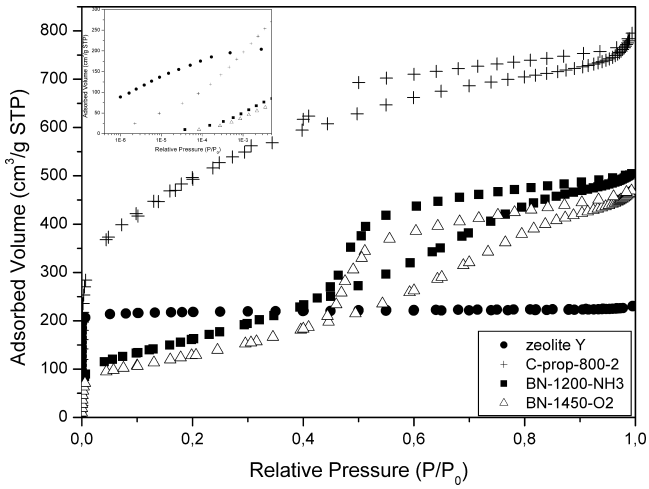

Figure 4. Nitrogen physisorptions at 77 K for zeolite Y, carbon replica C, BN-1200-NH_3 and BN-1450-O_2 materials.

On the basis of the isotherm profile, the zeolite **Y** is confirmed to be purely microporous (type I isotherm), whereas its carbonaceous replica displayed type I and IV components. This indicated both a microporous and a mesoporous features and the pore volumes have been calculated to be 0.7 and 0.5 cm^3/g, respectively. The bimodal pore size distribution (PSD), confirmed by NLDFT treatment (see the Supporting Information, Figure 1SI), is related to the preparation process. Here, the impregnation process in the gaseous phase (propylene) at 800 °C is not optimized for the carbon filling within the intracrystallite zeolite domains. After dissolution of the latter, voids corresponding to mesopores appeared associated also with collapsed domains. Therefore, in comparison to other gazeous

dx.doi.org/10.1021/cm201938h | *Chem. Mater.* 2012, 24, 88−96

carbon precursors such as acetylene[34] which leads to a highly microporous materials (1.2 cm^3/g) with nearly no mesopores (0.1 cm^3/g), the synthesis conditions used here provide a less porous and more broadly distributed porous material with a lower micropore volume (0.7 cm^3/g) and a higher portion of mesopores (0.5 cm^3/g instead of 0.1). The specific surface area (SSA) of the carbonaceous replica **C** is nevertheless high with 1700 m^2/g.

BN samples display type IV isotherms which are characteristic of mesoporous materials. The hysteresis loop of H2 type indicates that the samples are formed of a pore network of different sizes and shapes. BN samples display lower adsorbed volumes than the carbon replica, which is due to the presence of nonporous BN on the surface of the replicated BN observed by SEM and to collapsed-BN replicated domains. Nevertheless, relatively high SSA values are obtained for BN-based materials: 570 and 460 m^2/g for **BN-1200-NH$_3$** and **BN-1450-O$_2$** respectively. It is worth noting that these values have been obtained within the adequate relative pressure range (here 0.01−0.10) where the plot $(1-X)/X$ against $1/V(1-X)$, with V the volume adsorbed and X the relative pressure P/P_0, give a straight line.[51] Furthermore, both samples possess high pore volumes, 0.8 and 0.7 cm^3/g (at P/P_0 =0.95) for **BN-1200-NH$_3$** and **BN-1450-O$_2$**, respectively. For comparison, porous BN obtained by templating process using mesoporous carbon template[52,53] or based on reactive templating[54] have pore volume in the range 0.1 to 0.6 cm^3/g. Most of the time in the literature, a too large pressure range was taken for the determination of the specific surface area ($0.05 < P/P_0 < 0.3$) and consequently this latter is often overestimated. Again, the adequate pressure range is not constant for all materials and must be optimized each time to get the correct specific surface area.[51]

To determine if type I isotherm, characteristic of the presence of micropores, also contributes to the experimental BN isotherms, two different procedures have been followed. The former is based on the Dubinin−Raduskevitch (DR) theory,[55] whereas the second is based on the comparison of the experimental isotherms with a nonporous BN sample (*t*-plot method).[56] Because adsorption properties are very similar for both BN samples, only data related to **BN-1200-NH$_3$** sample are presented for sake of clarity. Adsorption isotherm redrawn based on the Dubinin−Radushkevich equation is reported in Figure 5.

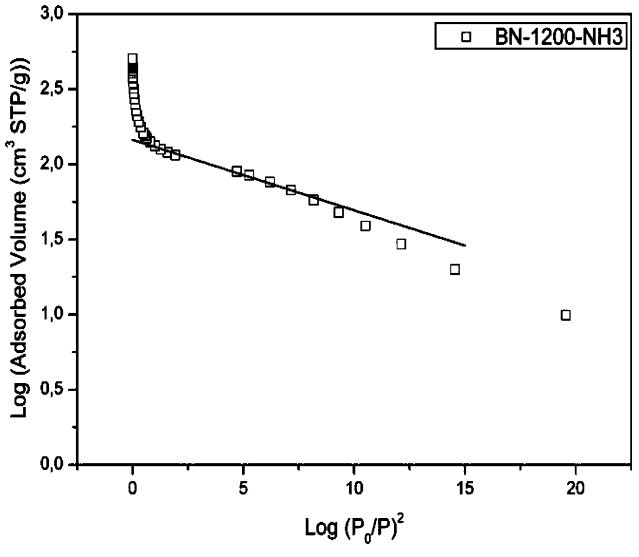

Figure 5. Dubinin−Radushkevich isotherms for the **BN-1200-NH$_3$** sample.

Intercept of the linear part of the plot with the ordinate axis gives micropore volume of 0.20 cm^3/g for **BN-1200-NH$_3$** (0.16 cm^3/g for **BN-1450- O$_2$**). Upward deviation of the curves at low $\log(P_0/P)^2$ is due to capillary condensation in mesopores.

The second analysis of the adsorption data is based on *t*-plot method. The adsorption isotherm of the porous boron nitride was then drawn as a function of the multilayer thickness *t* calculated based on the nonporous BN reference material (Figure 6).

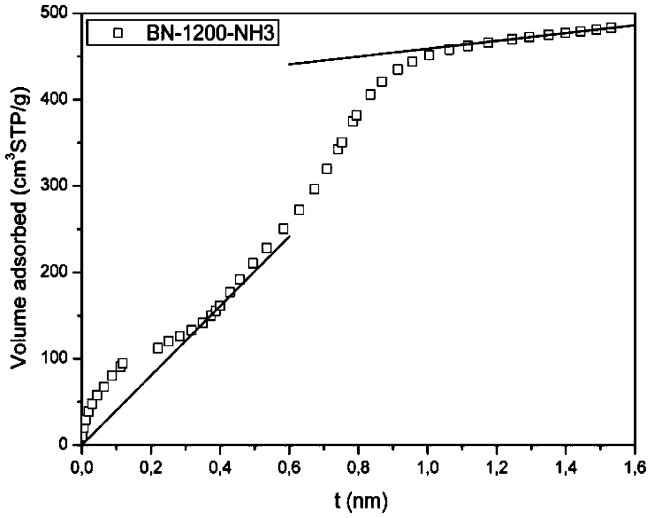

Figure 6. *t*-plot of the **BN-1200-NH$_3$** sample.

Because of the large pore size distribution continuously spreads over between the micro- and mesopore ranges, clear separation between both types of porosities is not straightforward. Nevertheless, three different domains can be distinguished according *t* values. To help the reader, a line passing through the origin and cutting the isotherm at t = 0.35 nm was plotted. For *t* below 0.35 nm ($P/P_0 < 0.15$), an upward swing is observed. It corresponds to a distortion of the isotherm due to enhanced adsorbant-absorbate interactions that take place in pores of molecular dimension (e.g.: primary micropore filling (pore size <0.8 nm). For *t* values in the range 0.35−1.0 nm ($0.15 < P/P_0 < 0.85$), the upward swing is here attributed to both a cooperative filling in secondary micropores (0.8 nm < pore size < 2 nm) and to a capillary condensation within the broadly distributed mesopore structure. At the completion of the mesopore filling, t > 1.0 nm ($0.85 < P/P_0 < 1$), unrestricted multilayer adsorption on the external surface area occurs. Its contribution to the total surface area has been estimated to 69 m^2/g.

The pore size distribution was determined by the DFT method (Figure 7).

Because of the absence of adapted kernel for BN materials, DFT approach developed for carbon materials with slitlike pores was used. Thus, one has to keep in mind that differences might exist between the real PSD and the calculated one. As previoulsy evidenced, a broad PSD of the sample with micro- and mesopores is observed. The contribution of micropores appears to be here close to 0.1 cm^3/g; this value is quite comparable to the 0.2 cm^3/g determined by the DR method, an analysis that is known to overestimate the micropore volume by taking into account the contribution of small mesopore.[56] Mesopores sizes extend up to 14 nm. The surface area determined by this technique with slitlike pore geometry is 400 and 340 m^2/g for **BN-1200-NH$_3$** and **BN-1450- O$_2$** samples, respectively.

dx.doi.org/10.1021/cm201938h | *Chem. Mater.* 2012, 24, 88−96

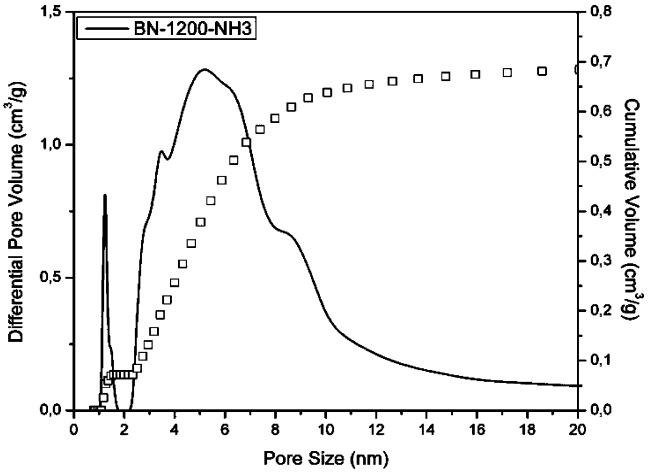

Figure 7. Pore size distributions obtained by DFT method (full line) and corresponding cumulative pore size distribution (square symbol) for the **BN-1200-NH$_3$** sample.

These different treatments of N_2 adsorption data (DR, t-plot) have unambiguously demonstrated for the first time, the presence of microporosity within BN-based materials.

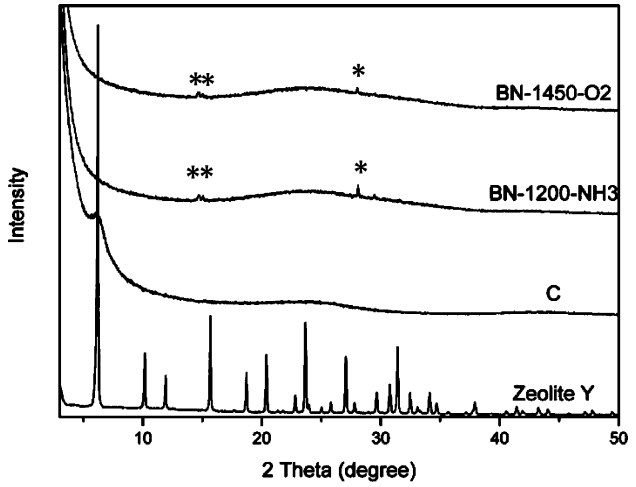

Figure 8. XRD patterns (Cu Kα radiation) of zeolite **Y**, carbon replica **C**, **BN-1200-NH$_3$**, and **BN-1450-O$_2$**. Small peaks labeled by a * correspond to boric acid $B(OH)_3$ (ICDD 00−030−0199).

XRD. X-ray diffraction diffractograms of the different samples are presented in Figure 8.

As expected, the zeolite **FAU Y** presents sharp peaks with significant intensities related to its crystalline nature in all the 2θ range. The carbonaceous replica **C** displays only one broad peak around 6.2° (2θ) at the same position of the most intense peak of the zeolite phase. This feature is well-known for zeolite-templated carbon replicas.[26,31] It indicates that a long-range ordering, with a periodicity around 1.34 nm arising from the zeolite template, is preserved. In contrast, both BN samples **BN-1200-NH$_3$** and **BN-1450-O$_2$** did not display peaks in this 2θ range indicating the lack of porosity organization after the double nanocasting process. Indeed, it is well-known in hard-templating[57] and more in "repeated templating"[58,59] that each step of the process leads to a progressive loss of structuration compare to the starting template due to a noncomplete filling of the template and/or a collapse of the replicated structure. This feature is here even more pronounced with microporous templates difficult to infiltrate. The degree of organization (at the nanometric scale) decreases and appears then, after the second step, to be undetectable with XRD technique, which is a technique sensitive to the long-range ordering. More surprisingly is the absence of crystallization for BN-based materials (here at the atomic scale) even after high temperature-treatment (1450 °C). This phenomena was also confirmed by HRTEM (see below). The origin of this unusual behavior could be attributed to the nanoconfinement of BN material within the porosity of the zeolite-templated carbon replica. This porosity (mainly micropores) is lower than those of mesostructured carbon-templates used in previous studies (e.g., CMK-3); it could preclude the crystallization of the material on a long−range scale detectable by XRD. Similar features have already been encountered for nanostructured carbons synthesized in confined media by hard-templating technique.[60] It was shown that steric limitations imposed by the template's mesoporosity lead to misorientation of carbon-structural units; the absence of preoriented graphene domains preclude then their layer stacking and the carbon materials did not graphitized easily compared to bulk samples prepared in similar conditions. Such behavior could occur in the case of our BN-based materials.

As previously mentioned, these samples contain a significant amount of oxygen. Its presence is partly evidenced by XRD (see Figure 8) with traces of boric acid ($B(OH)_3$). Oxygen has shown to promote crystallization of bulky BN[61] but this trend appears not to happen here probably because of the strong confinement effect.

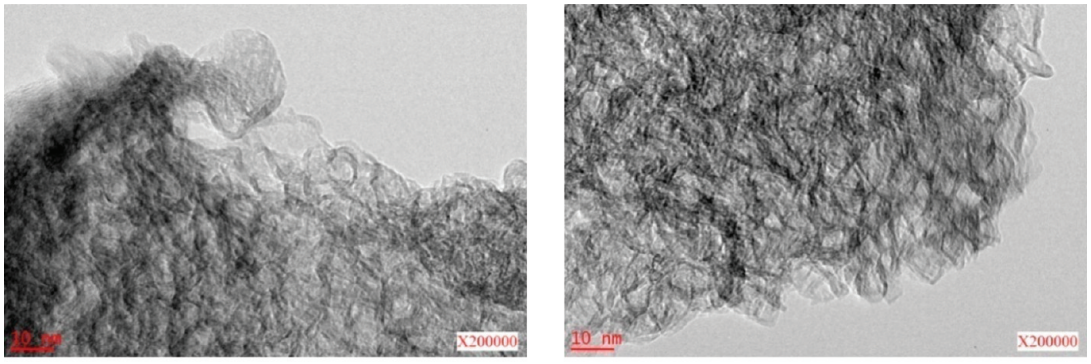

(a) (b)

Figure 9. HRTEM images of (a) BN-1200-NH$_3$ and (b) BN-1450-O$_2$.

dx.doi.org/10.1021/cm201938h | *Chem. Mater.* 2012, 24, 88−96

Transmission Electronic Microscopy (TEM). TEM (Figure 9) performed on the two BN samples highly reflected BET and XRD results.

Both samples appeared to be relatively highly porous without long-range nano-ordering and crystalline domains. We can especially distinguish a nanostructure made of porous nano-polyhedral shapes with a pore size of about 5−10 nm and a very thin shell thickness (1−2 nm).

CONCLUSION

In summary, amorphous boron nitride-based porous materials have been obtained by a double nanocasting process starting from zeolite in which we sequenced several synthetic strategies coupling chemical vapor deposition (CVD) and Polymer-Derived Ceramic (PDCs) routes. In a first step, we prepared carbonaceous templates through infiltration of Zeolite FAU Y by propylene in the gaseous phase before dissolution of zeolite in HF and, in a second step, we infiltrated the carbonaceous replica having a high micropore volume (0.67 cm^3/g) with polyborazylene in the liquid phase followed by pyrolysis and mold destruction. These porous BN-based architectures are amorphous. This unusual amorphous behavior is attributed to the confinement of BN materials within the nanometric porosity of the zeolite-templated carbonaceous replica. They display a bimodal pore size distribution with a high pore volume (0.78 cm^3/g) and a high portion of micropores (~0.20 cm^3/g) and specific surface areas up to 570 m^2/g. The unique combination of the properties of the proposed porous structure, i.e., low density, high geometric surface area, permeability, and dimensional stability with the intrinsic properties of BN such as thermal shock resistance, thermal conductivity, dielectric constant, and resistance to chemical corrosion and molten metals render this class of porous architectures promising for specific functional purposes of significant interest such as filtration membranes, catalyst carriers, and even scaffolds for bone replacement. In particular, these porous BN can be shaped directly into monolith or honeycomb forms including some catalytically active material. Furthermore, they could be modified for specific catalytic applications through the addition of metals. We think that such porous BN are used as support of transition metals to elaborate homogeneous or heterogeneous catalysts[62,63] that make dehydrogenation of chemical hydrides by thermolysis or solvolysis milder, respectively. Besides, in thermolysis, BN acts as an ideal host of hydrides such as ammonia borane, in which dehydrogenation can then occur at lower temperatures than that observed for the pristine material.[64] Such a study is under investigation and will be published separately.

ASSOCIATED CONTENT

Supporting Information

Pore size distribution of C replica. Experimental conditions of the ceramization and carbon removal treatments with corresponding residual carbon content. Correspondences between t and P/P_0 for a nonporous BN reference material. This material is available free of charge via the Internet at http://pubs.acs.org.

AUTHOR INFORMATION

Corresponding Author

*Tel.: +33 3 89 60 87 02 (J.P.); +33 467 149 181 (S.B.). Fax: +33 3 89 60 87 99 (J.P.); +33 467 149 119 (S.B.). E-mail: julien.parmentier@univ-mulhouse.fr; (J.P.) Samuel.Bernard@iemm.univ-montp2.fr (S.B.).

ACKNOWLEDGMENTS

We are grateful to the Agence Nationale de la Recherche (ANR) for supporting this research program through the ANR-08-BLAN-0189-01 contract.

REFERENCES

(1) Paine, R. T.; Narula, C. K. *Chem. Rev.* **1990**, *90*, 73.
(2) Wu, J.; Han, W. Q.; Walukiewicz, W; Ager, J. W. III; Shan, W.; Haller, E. E.; Zettl, A. *Nano Lett.* **2004**, *4*, 647.
(3) Watanabe, K.; Tanigushi, T.; Kanda, H. *Nat. Mater.* **2004**, *3*, 404.
(4) Kubota, Y.; Watanabe, K.; Tsuda, O.; Tanigushi, T. *Science* **2007**, *317*, 932.
(5) Macnaughton, J. B.; Moewes, A.; Wilks, R. G.; Zhou, X. T.; Sham, T. K.; Tanigushi, T.; Watanabe, K.; Chan, C. Y.; Zhang, W. J.; Bello, I.; Lee, S. T. *Phys. Rev. B* **2005**, *72*, 195113.
(6) Riedel, R.; Mera, G.; Hauser, R.; Klonczynski, A. *J. Ceran. Soc. Jpn.* **2006**, *114*, 425.
(7) Colombo, P.; Soraru, G. D.; Riedel, R.; Kleebe, H. J. *DEStech Publications, Inc.* **2009**, 410.
(8) Colombo, P.; Mera, G.; Riedel, R.; Soraru, G. D. *J. Am. Ceram. Soc.* **2010**, *93*, 1805.
(9) Miele, P.; Bernard, S.; Cornu, D.; Toury, B. *Soft. Mater.* **2006**, *4*, 249.
(10) P. Toutois, P.; Miele, P.; Jacques, S.; Cornu, D.; Bernard, S. *J. Am. Ceram. Soc.* **2006**, *89*, 42.
(11) Duperrier, S.; Chiriac, R.; Sigala, C.; Gervais, C.; Bernard, S.; Cornu, D.; Miele, P. *J. Eur. Ceram. Soc.* **2009**, *29*, 851.
(12) http://www.clariant.com
(13) http://www.dowcorning.com
(14) http://www.starfiresystems.com
(15) Lin, L.; Li, Z.; Zheng, Y.; Wei, K. *J. Am. Ceram. Soc.* **2009**, *92*, 1347.
(16) Han, W.-Q.; Brutchey, R.; Tilley, T. D.; Zettl, A. *Nano Lett.* **2004**, *4*, 173.
(17) Dibandjo, P.; Bois, L.; Chassagneux, F.; Cornu, D.; Létoffé, J. M.; Toury, B.; Babonneau, F.; Miele, P. *Adv. Mater.* **2005**, *17*, 571.
(18) Yan, J.; Wang, A. J.; Kim, D. P. *J. Phys. Chem. B* **2006**, *110*, 5429.
(19) Nghiem, Q. D.; Kim, D.; Kim, D. P. *Adv. Mater.* **2007**, *19*, 2351.
(20) Shi, Y.; Wan, Y.; Tu, B.; Zhao, D. *J. Phys. Chem. C* **2008**, *112*, 112.
(21) Krawiec, P.; Geiger, D.; Kaskel, S. *Chem. Commun.* **2006**, 2469.
(22) Majoulet, O.; Alauzun, J. G.; Gottardo, L.; Gervais, C.; Schuster, M. E.; Bernard, S.; Miele, P. *Microporous Mesoporous Mater.* **2011**, *140*, 40.
(23) Wang, H.; Li, X. D.; Yu, J. S.; Kim, D. P. *J. Mater. Chem.* **2004**, *14*, 1383.
(24) Yan, X. B.; Gottardo, L.; Bernard, S.; Dibandjo, P.; Brioude, A.; Moutaabbid, H.; Miele, P. *Chem. Mater.* **2008**, *20*, 6325.
(25) Kyotani, T.; Nagai, T.; Tomita, A. *Extended Abstracts of Carbon'92*, Essen, Germany,1992; p 437.
(26) Kyotani, T.; Nagai, T.; Inoue, S.; Tomita, A. *Chem. Mater.* **1997**, *9*, 609.
(27) Kyotani, T.; Ma, Z.; Tomita., A. *Carbon* **2003**, *41*, 1451.
(28) Tosheva, L.; Parmentier, J.; Valtchev, V.; Vix-Guterl, C.; Patarin, J. *Carbon* **2005**, *43*, 2474.
(29) Parmentier, J.; Valtchev, V.; Gaslain, F.; Tosheva, L.; Ducrot-Boisgontier, C.; Möller, J.; Patarin, J.; Vix-Guterl, C. *Carbon* **2009**, *47*, 1066.
(30) Gaslain, F.; Parmentier, J.; Valtchev, V.; Patarin, J. *Chem. Commun.* **2006**, 991.
(31) Ducrot-Boisgontier, C.; Parmentier, J.; Patarin, J. *Microporous Mesoporous Mater.* **2009**, *126*, 101.
(32) Ducrot-Boisgontier, C.; Parmentier, J.; Delmotte, L.; Patarin, J. *J. Mater. Sci.* **2009**, *44*, 6571.
(33) Xia, Y.; Mokaya, R.; Grant, D. M.; Walker, G. S. *Carbon* **2011**, *49*, 844.
(34) Ducrot-Boisgontier, C.; Parmentier, J.; Faour, A.; Patarin, J.; Pirngruber, G. D. *Energy Fuels* **2010**, *24*, 3595.

(35) Yang, Z. X.; Xia, Y. D.; Sun, X. Z.; Mokaya, R. *J. Phys. Chem. B* **2006**, *110*, 18424.
(36) Bechelany, M.; Bernard, S.; Brioude, A.; Cornu, D.; Stadelmann, P.; Charcosset, C.; Fiaty, K.; Miele, P. *J. Phys. Chem. C* **2007**, *111*, 13378.
(37) Massiot, D.; Fayon, F.; Capron, M.; King, I.; Le Calvé, S.; Alonso, B.; Durand, J.; Bujoli, B.; Ghan, Z.; Hoatson, G. *Magn. Reson. Chem.* **2002**, *20*, 70.
(38) Brunauer, S.; Emmett, P. H.; Teller, E. *J. Am. Chem. Soc.* **1938**, *60*, 309.
(39) Carrotta, P. J. M.; Mc-Leod, A. I.; Sing, K. S. W. *Stud. Surf. Sci. Catal.* **1982**, *10*, 403.
(40) Lippens, B. *J. Catal.* **1965**, *4*, 319.
(41) Ma, Z.; Kyotani, T.; Tomita, A. *Carbon* **2002**, *40*, 2367.
(42) Nishihara, H.; Yang, Q.-H.; Hou, P.-X.; Unno, M.; Yamauchi, S.; Saito, R.; Paredes, J. I.; Martínez-Alonso, A.; Tascón, J. M. D.; Sato, Y.; Terauchi, M.; Kyotani, T. *Carbon* **2009**, *47*, 1220.
(43) (a) Salles, V.; Bernard, S.; Li, J. J.; Brioude, A.; Chehaidi, S.; Foucaud, S.; Miele, P. *Chem. Mater.* **2009**, *21*, 2920. (b) Bernard, S.; Salles, V.; Li, J.; Brioude, A.; Bechelany, M.; Demirci, U. B.; Miele, P. *J. Mater. Chem.* **2011**, *21*, 8694.
(44) Li, J.; Bernard, S.; Salles, V.; Gervais, C.; Miele, P. *Chem. Mater.* **2010**, *22*, 2010.
(45) Duperrier, S.; Gervais, C.; Bernard, S.; Cornu, D.; Babonneau, F.; Miele, P. *J. Mater. Chem.* **2006**, *16*, 3126.
(46) Marchetti, P. S.; Kwon, D.; Schmidt, W. R.; Interrante, L. V.; Maciel, G. E. *Chem. Mater.* **2002**, *3*, 482.
(47) Gervais, C.; Maquet, J.; Babonneau, F.; Duriez, C.; Framery, E.; Vaultier, M.; Florian, P.; Massiot, D. *Chem. Mater.* **2001**, *13*, 1700.
(48) Irwin, A. D.; Holmgren, J. S.; Jonas, J. *J. Non-Cryst. Solids* **1988**, *101*, 249.
(49) Van Wüllen, L.; Müller-Warmuth, W. *Solid State NMR* **1993**, *2*, 279.
(50) Soraru, G. D.; Dallabona, N.; Gervais, C.; Babonneau, F. *Chem. Mater.* **1999**, *11*, 910.
(51) Parra, J. B.; de Sousa, J. C.; Bansal, R. C.; Pis, J. J.; Pajares, J. A. *Adsorption Science and Technology* **1995**, *12*, 51.
(52) Dibandjo, P.; Chassagneux, F.; Bois, L.; Sigala, C.; Miele, P. *J. Mater. Chem.* **2005**, *15*, 1917.
(53) Dibandjo, P.; Chassagneux, F.; Bois, L.; Sigala, C.; Miele, P. *Microporous Mesoporous Mater.* **2006**, *92*, 286.
(54) Rushton, B.; Mokaya, R. *J. Mater. Chem.* **2008**, *18*, 235.
(55) Hutson, N. D.; Yang, R. T. *Adsorption* **1997**, *3*, 189.
(56) Rouquerol, F.,; Rouquerol, J. ; Sing, K. S. W. *Adsorption by Powders and Porous Solids*; Academic Press: London, 2000.
(57) Marsh, H.; Rodriguez-Reinoso, F. *Activated Carbon*; Elsevier Science & Technology Books: Amsterdam, 2006; p 180.
(58) Parmentier, J.; Saadhallah, S.; Reda, M.; Gibot, P.; Roux, M.; Vidal, L.; Vix-Guterl, C.; Patarin, J. *J. Phys. Chem. Solids* **2004**, *65*, 139.
(59) Tiemann, M. *Chem. Mater.* **2008**, *20*, 961.
(60) Parmentier, J.; Vix-Guterl, C.; Saadallah, S.; Reda, M.; Illescu, M.; Werckmann, J.; Patarin, J. *Chem. Lett.* **2003**, *3*, 262.
(61) Gadiou, R.; Didion, A.; Saadallah, S.-E.; Couzi, M.; Rouzaud, J.-N.; Delhaes, P.; Vix-Guterl, C. *Carbon* **2006**, *44*, 3348.
(62) Demirci, U. B.; Akdim, O.; Andrieux, J.; Hannauer, J.; Chamoun, R.; Miele, P. *Fuel Cells* **2010**, *10*, 335.
(63) Demirci, U. B.; Bernard, S.; Chiriac, R.; Toche, F.; Miele, P. *J. Power Sources* **2011**, *196*, 279.
(64) Neiner, D.; Karkamkar, A.; Linehan, J. C.; Arey, B.; Autrey, T.; Kauzlarich, S. M. *J. Phys. Chem. C* **2009**, *113*, 1098.